

## Supporting Information

### **Selectivity anchoring Pt NPs on covalent triazine-based frameworks via *in-situ* derived bridging ligands for boosting photocatalytic hydrogen evolution**

Ling-Ling Zheng,<sup>a,b</sup> Xiang Li,<sup>b,c</sup> Ying Chen,<sup>a,b</sup> Qian Fu,<sup>a,b</sup> Dai-She Wu,<sup>a</sup> Xiao-Zhen Liu,<sup>\*a</sup> and Jian-Ping Zou<sup>\*a,b</sup>

*a* Key Laboratory of Poyang Lake Environment and Resource Utilization of Ministry of Education, School of Resources Environmental and Chemical Engineering, Nanchang University, Nanchang 330031, P. R. China

*b* National-Local Joint Engineering Research Center of Heavy Metals Pollutants Control and Resource Utilization, Nanchang Hangkong University, Nanchang 330063, P. R. China

*c* Jiangxi Key Laboratory of Environmental Pollution Control, Jiangxi Academy of eco-environmental Sciences and Planning, Nanchang 330063, P. R. China

## Characterizations

X-ray diffraction (XRD) patterns were collected on a D8 Advance X-ray diffractometer (Bruker, Germany) with Cu K $\alpha$  radiation. Fourier Translation Infrared spectroscopy (FTIR) was recorded on a Nicolet 410 FTIR spectrometer. The morphology of the catalysts was measured via scanning electron microscopy (SEM, FEI, Hillsboro, OR, USA), transmission electron microscopy (TEM, JEOL model JEM 2010 EX instrument) and high-resolution transmission electron microscopy (HRTEM). UV-visible diffuse reflectance spectra (UV-vis DRS) of the powders were obtained with BaSO<sub>4</sub> used as a reflectance standard. X-ray photoelectron spectroscopy (XPS) measurements were performed on a PHI Quantum 2000 XPS system (PHI, USA). Photoluminescence (PL) spectra were carried out on a fluorescence spectrometer (Hitachi F-4500) with 340 nm as the excitation wavelength. Time-resolved fluorescence decay spectra (TPRL, FS5 Spectrofluorometer, excitation source of 380 nm picosecond pulsed diode laser) were collected to investigate the fluorescence and fluorescent lifetime of the samples. Solid-state <sup>13</sup>C cross-polarization (CP)/magic-angle-spinning (MAS) nuclear magnetic resonance (NMR) spectra were obtained using a Bruker AVANCE-III spectrometer. Raman spectra were obtained on an invite-reflex micro-Raman spectroscopy system (Renishaw Co.) with a 633 nm line of an Ar ion laser at room temperature. The contents of Pt in the Pt/1.0%AT-CTF-1 under different loading content of Pt were measured from the inductively coupled plasma-optical emission spectrometer (ICP-OES, Perkin Elmer, Elmer Optima 2000DV). Electrochemical impedance spectroscopy and light current were measured on an electrochemical analyzer (Zahner, Germany) in a standard three-electrode system using the prepared samples as the working electrode, a platinum wire as the counter electrode, and Ag/AgCl (saturated KCl) as a reference electrode. Na<sub>2</sub>SO<sub>4</sub> (0.5 M) was used as electrolyte. As for photocurrent measurements, a 300 W Xe lamp (Perfect light PLS-SXE300C) was used as the source of simulated solar irradiation and the other conditions were the same as those of electrochemical measurements.

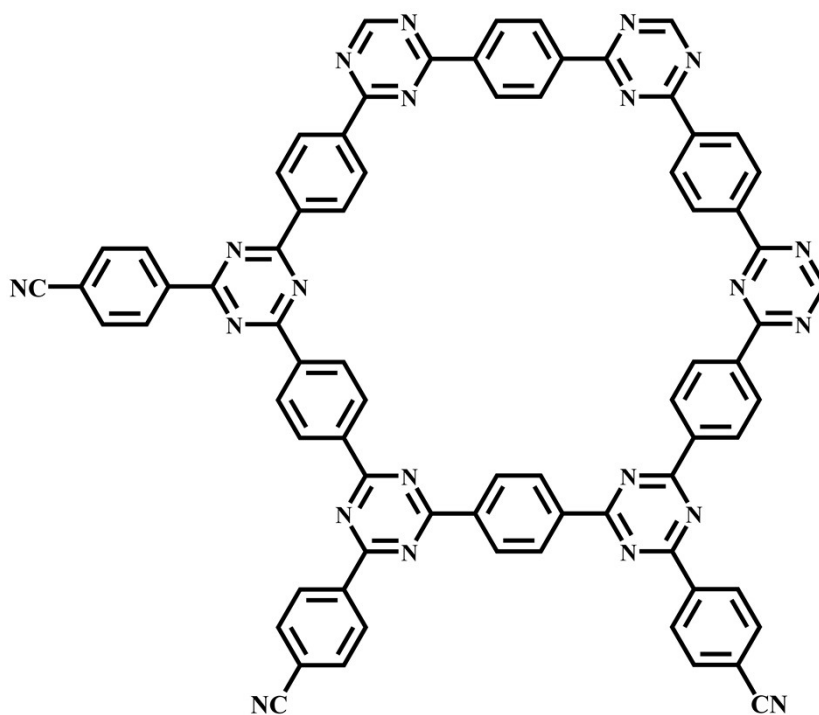


**Fig. S1** The structure diagram of the CTF-1.

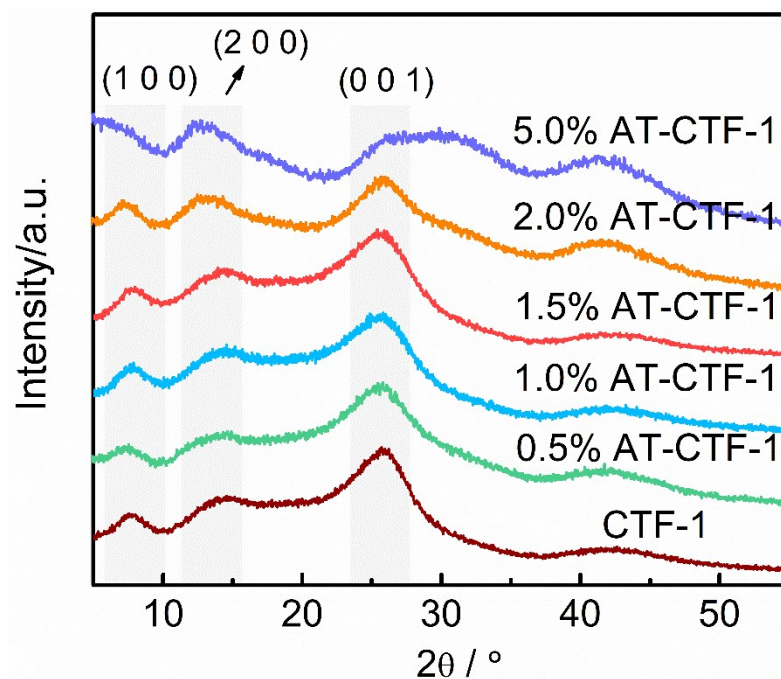


**Fig. S2** The XRD patterns of the AT-CTF-1 treated with different contents of NaOH.

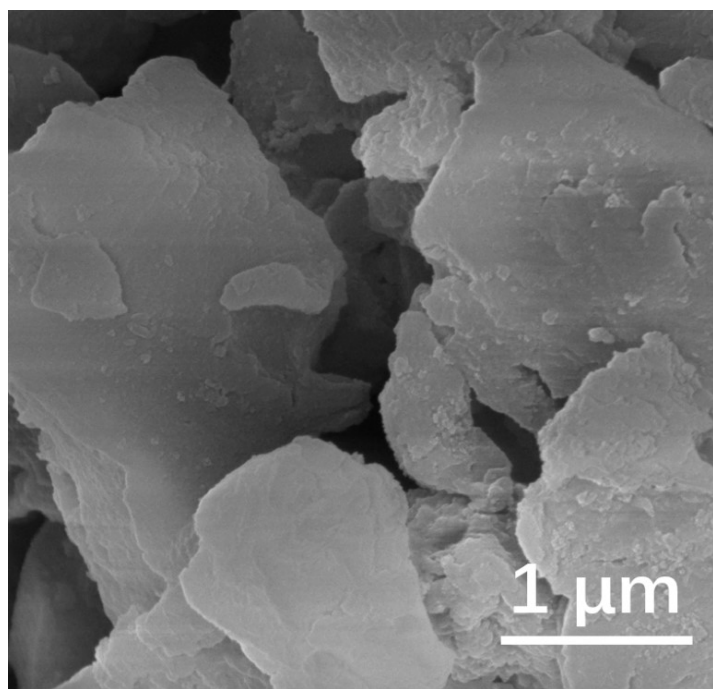


**Fig. S3** The SEM of the pure CTF-1.

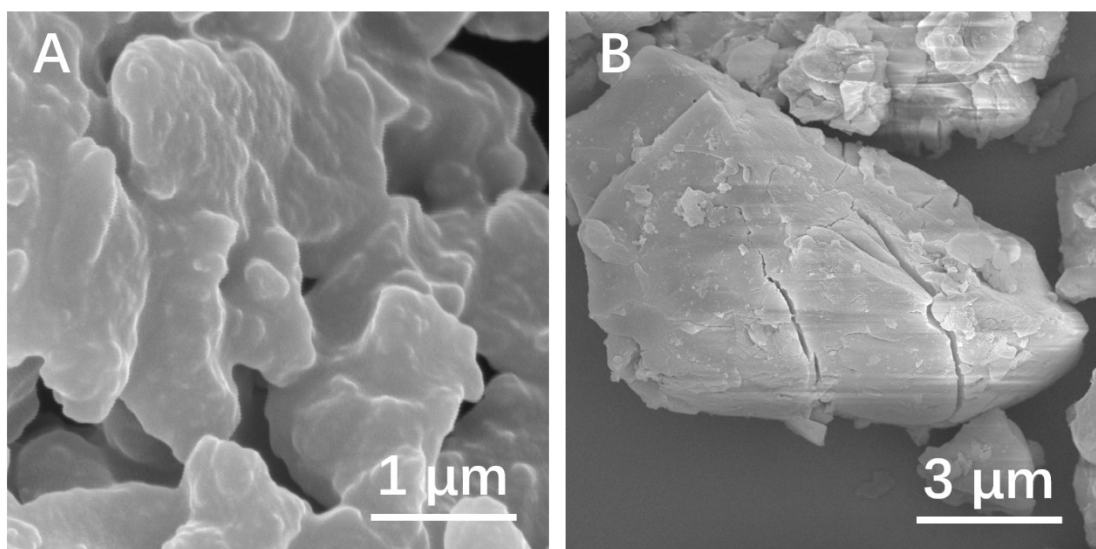


**Fig. S4** The SEM of the (a) 1.0%AT-CTF-1 and (b) 5.0%AT-CTF-1.

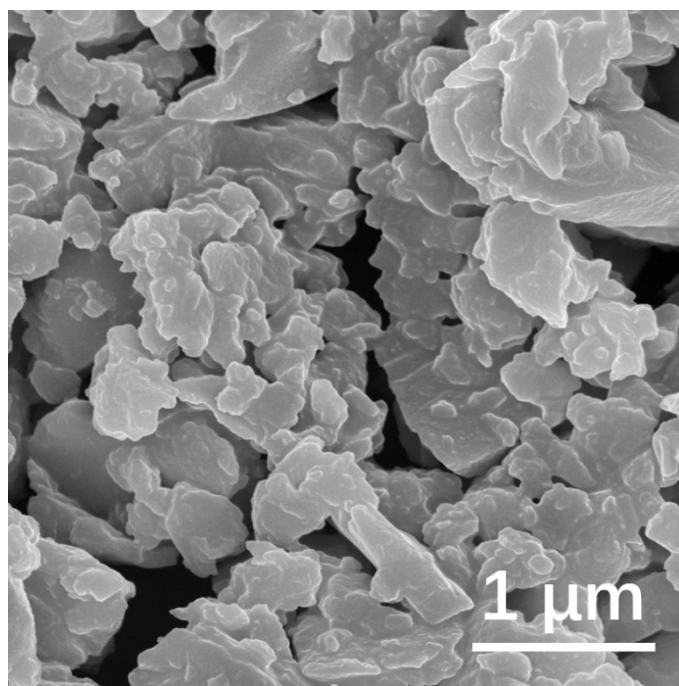


**Fig. S5** The SEM of the pure Pt/AT-CTF-1.

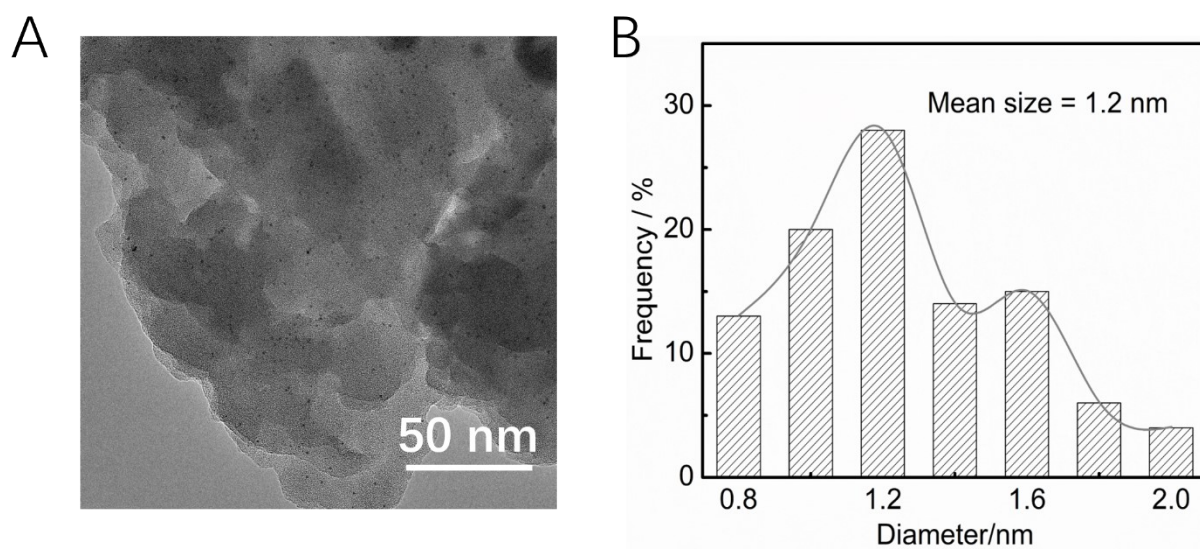


**Fig. S6** (a) TEM image and (b) Pt nanoparticles size distribution histogram of the Pt/AT-CTF-1.

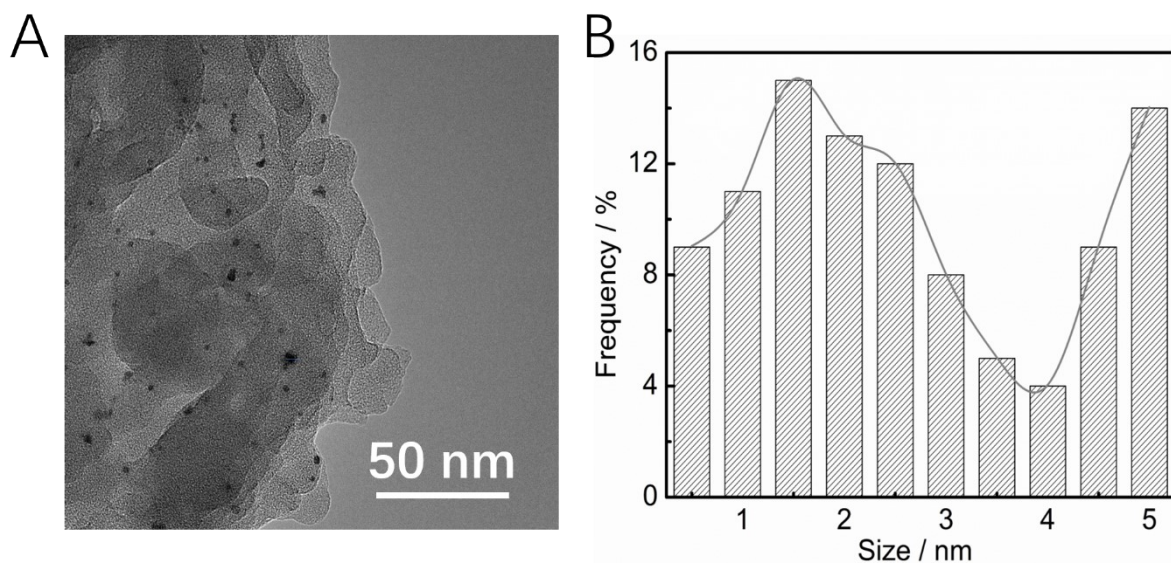


**Fig. S7** (a) TEM image and (b) Pt nanoparticles size distribution histogram of the Pt/CTF-1.

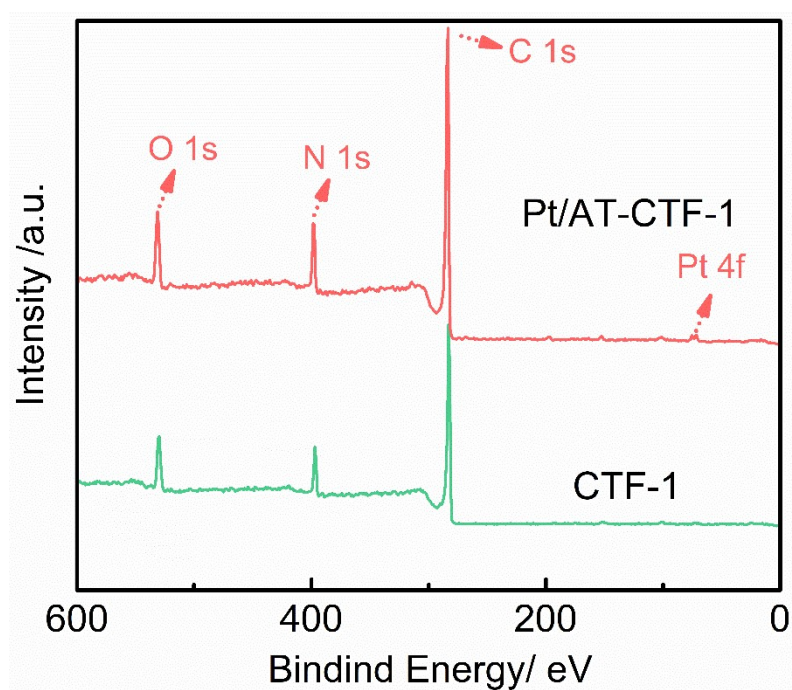


**Fig. S8** XPS spectra of the survey scan of CTF-1 and Pt/AT-CTF-1.

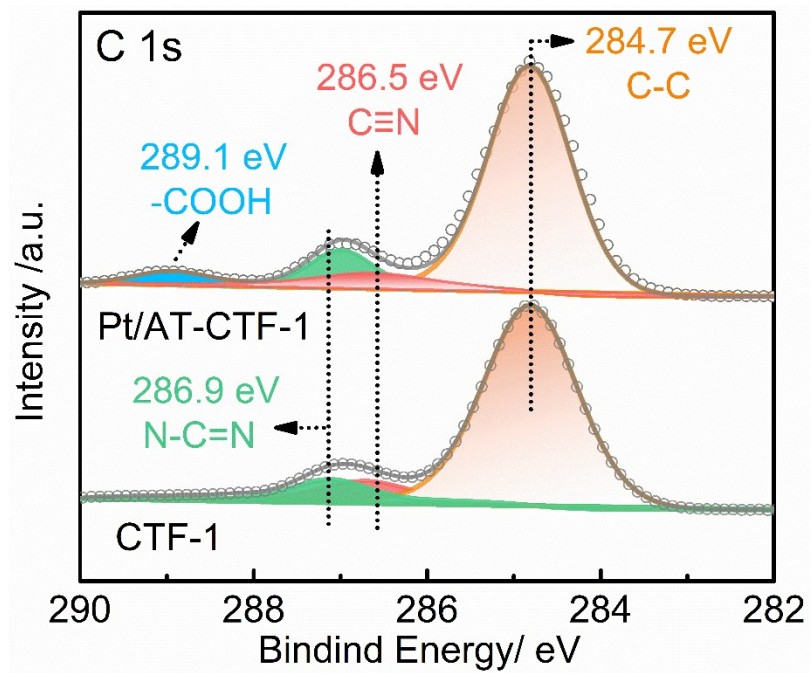


**Fig. S9** XPS spectra of C 1s of CTF-1 and AT-CTF-1.

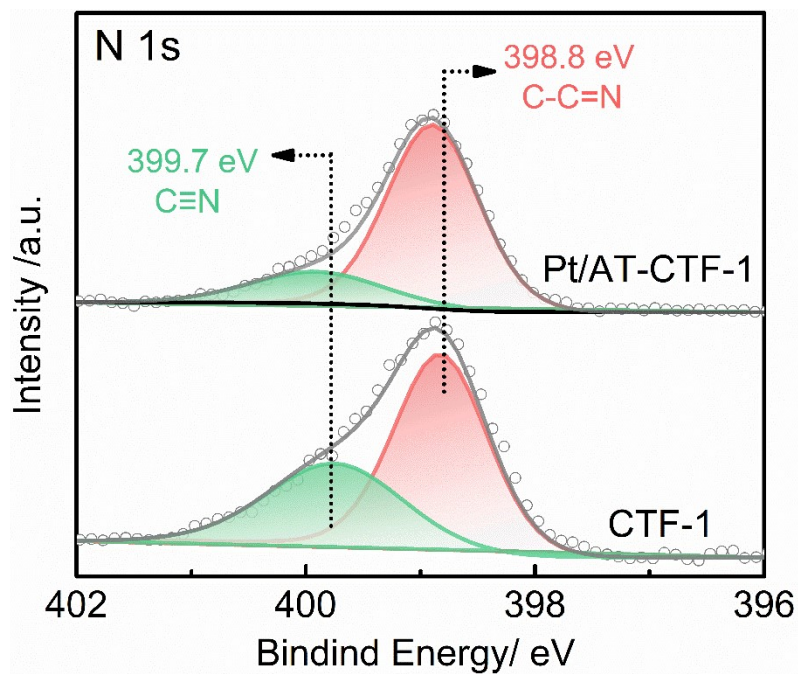


**Fig. S10** XPS spectra of N 1s of CTF-1 and Pt/AT-CTF-1.

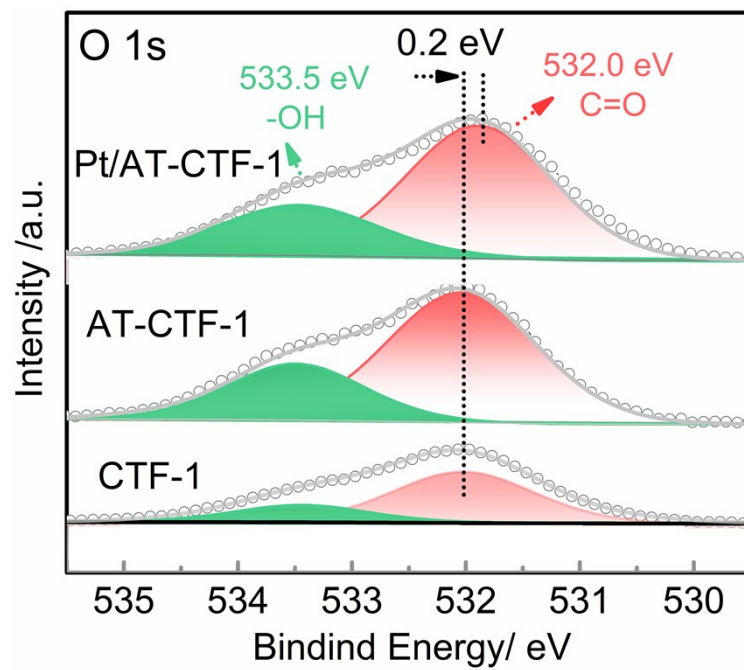


**Fig. S11** XPS spectra of O 1s of the as-prepared materials.

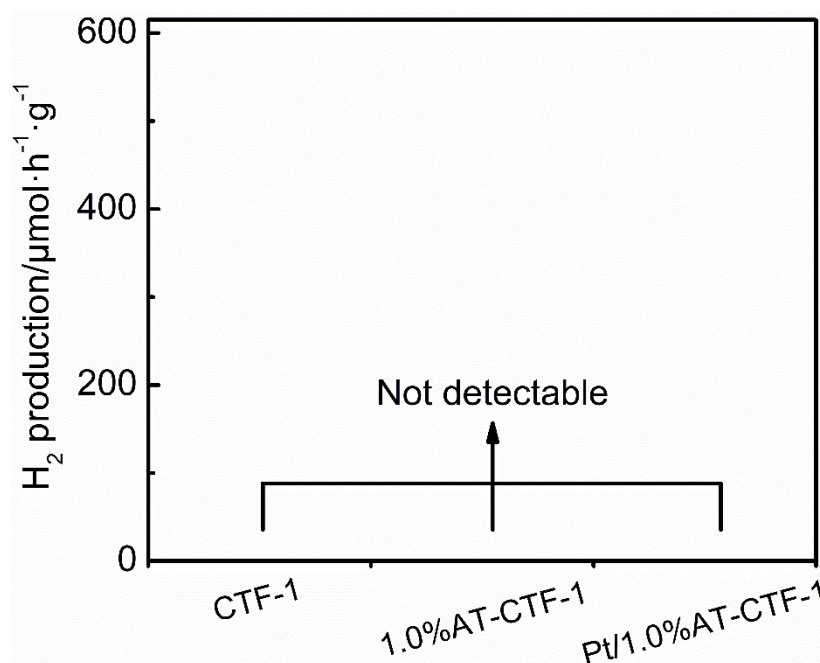


**Fig. S12** Photocatalytic  $H_2$  evolution rate of CTF-1, 1.0%AT-CTF-1 and Pt/1.0%AT-CTF-1 under dark.

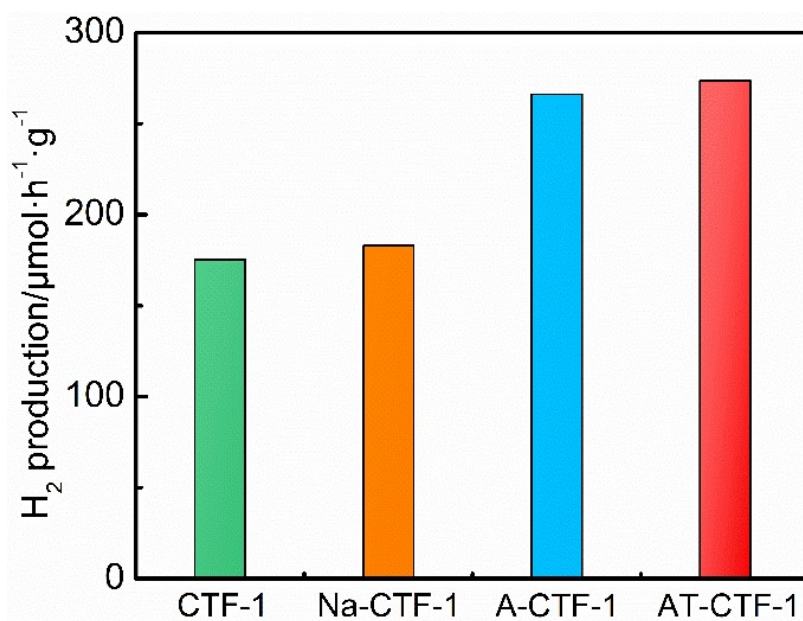


**Fig. S13** The H<sub>2</sub> evolution over the CTF-1, Na-CTF-1, A-CTF-1 and AT-CTF-1.

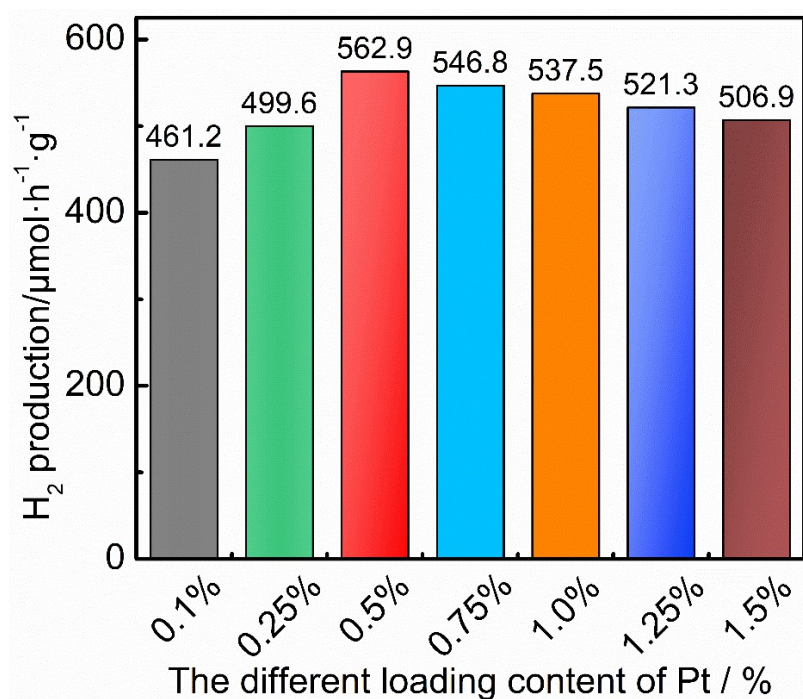


**Fig. S14** Photocatalytic H<sub>2</sub> evolution rate of the Pt/1.0%AT-CTF-1 under different loading content of Pt.

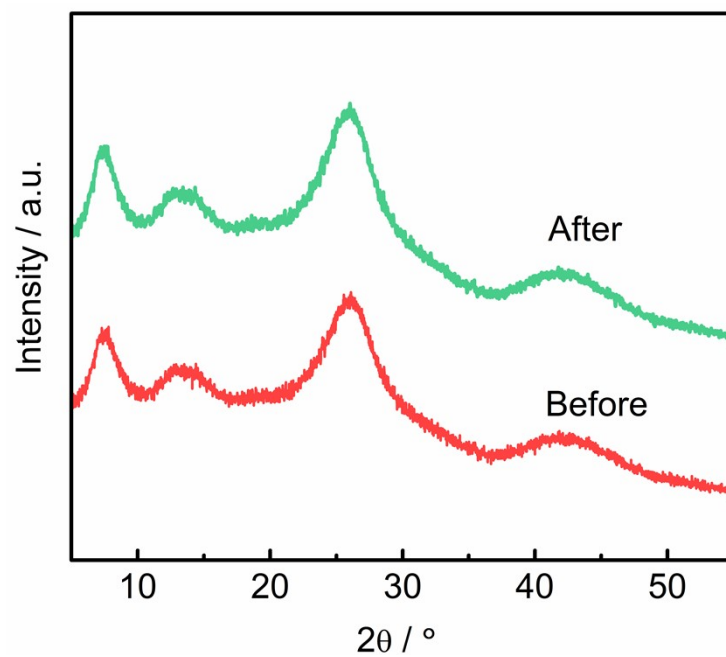


**Fig. S15** XRD patterns of the Pt/AT-CTF-1 before and after the reaction.

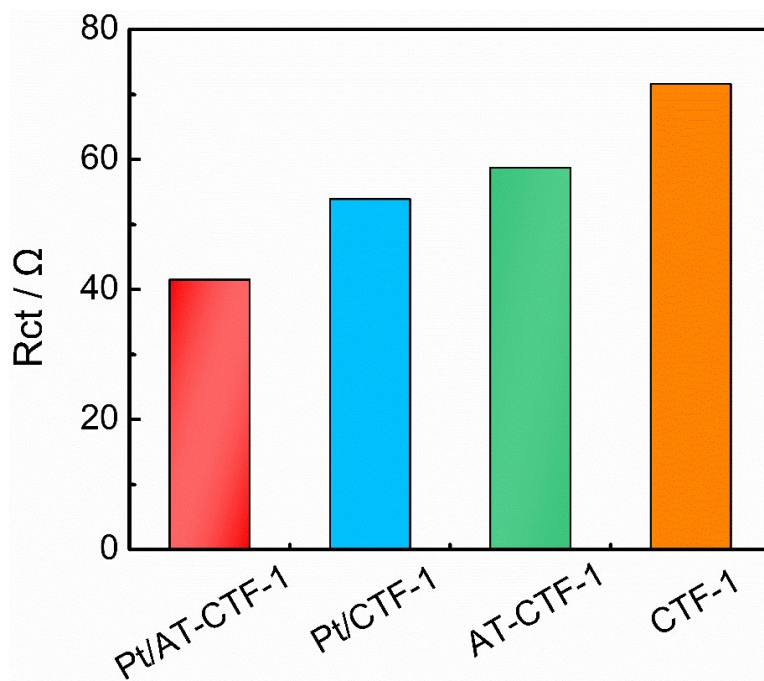


**Fig. S16** The charge-transfer resistance of CTF-1, AT-CTF-1, Pt/CTF-1 and Pt/AT-CTF-1.

**Table S1.** Exponential decay-fitted parameters of fluorescence lifetime for the CTF-1, AT-CTF-1, Pt/CTF-1 and Pt/AT-CTF-1 samples.

Sample	$\tau_1$ / ns	$\tau_2$ / ns	$\tau_{ave}$ / ns
CTF-1	0.21	3.07	1.36
AT-CTF-1	0.25	3.25	1.58
Pt/CTF-1	0.32	3.51	1.82
Pt/AT-CTF-1	0.47	4.16	<b>2.24</b>

The average lifetime ( $\tau_{ave}$ ) was calculated using the following equation:

$$\tau_{ave} = \frac{\tau_1^2 A_1 + \tau_2^2 A_2}{\tau_1 A_1 + \tau_2 A_2}$$

where  $\tau_1$ , and  $\tau_2$  are the emission lifetimes, and  $A_1$  and  $A_2$  are the corresponding amplitudes. In general, the longer decay lifetime component  $\tau_1$  is considered to free exciton recombination in the catalysts, and the shorter decay lifetime components  $\tau_2$  are ascribed to the surface-related nonradiative recombination of the charge carriers.